

Dynamics of potential vorticity staircase evolution and step mergers in a reduced model of beta-plane turbulence

M. A. Malkov¹ and P. H. Diamond^{1,2}

¹CASS and Department of Physics, University of California, San Diego, California 92093, USA

²Center for Fusion Sciences, Southwestern Institute of Physics, Chengdu, Sichuan 610041, People's Republic of China



(Received 30 November 2018; published 22 April 2019)

A two-field model of potential vorticity (PV) staircase structure and dynamics relevant to both beta-plane and drift-wave plasma turbulence is studied numerically and analytically. The model evolves averaged PV whose flux is both driven by and regulates a potential enstrophy field, ε . The model employs a closure using a mixing length model. Its link to bistability, vital to staircase generation, is analyzed and verified by integrating the equations numerically. Long-time staircase evolution consistently manifests a pattern of metastable quasiperiodic configurations, lasting for hundreds of time units, yet interspersed with abrupt ($\Delta t \ll 1$) mergers of adjacent steps in the staircase. The mergers occur at the staircase lattice defects where the pattern has not completely relaxed to a strictly periodic solution that can be obtained analytically. Other types of stationary solutions are solitons and kinks in the PV gradient and ε -profiles. The waiting time between mergers increases strongly as the number of steps in the staircase decreases. This is because of an exponential decrease in interstep coupling strength with growing spacing. The long-time staircase dynamics is shown numerically to be determined by local interaction with adjacent steps. Mergers reveal themselves through the explosive growth of the turbulent PV flux, which, however, abruptly drops to its global constant value once the merger is completed.

DOI: [10.1103/PhysRevFluids.4.044503](https://doi.org/10.1103/PhysRevFluids.4.044503)

I. INTRODUCTION

Pattern and scale selection are omnipresent problems in the dynamics of fluids and related nonlinear continuum systems. In geophysical fluids, as described by the beta-plane [1] or quasigeostrophic equations [2], the mechanisms of formation and scale selection for arrays of jets or zonal flows [3] are of particular interest. The jets scale constitutes an emergent scale which often defines the extent of mixing, transport, and other important physical phenomena. Beta-plane and quasigeostrophic systems evolve by the Lagrangian conservation of potential vorticity (PV). The latter is an effective phase space density which consists of the sum of planetary and fluid pieces. The question of scale selection then is inexorably wrapped up in the evolution of *mixing* of PV. Homogeneous mixing, predicted by the Prandtl-Batchelor theorem [1–3], leads to a uniform PV profile throughout the system with a sharp PV gradient at the boundary. Inhomogeneous mixing is linked to bistability of mixing, multiscale PV patterns. One of these, a corrugated structure called the *potential vorticity staircase*, is of particular interest, as it is a long-lived, quasistationary pattern of jets. The struggle between homogenization and (homogeneous mixing) and corrugation (inhomogeneous mixing) of PV is central to the dynamics of staircase formation and evolution, which are the foci of this paper.

The turbulent transport and structure formation phenomenon now commonly known as a “staircase” was first understood and described by Philips [4]. He considered a density profile in the ocean that, being stably stratified overall, occasionally reorganizes itself into layers separated by thin interfaces. The density gradient flattens in the layers and steepens in the interfaces (sheets). Thus,

an initially linear density profile becomes *ragged*, hence the name “staircase.” An interesting aspect of the Phillips paradigm, by which it can be distinguished from other pattern formation scenarios in (nonlinear) unstable media, is the preexisting turbulent transport mechanism that is both supported by, and regulates, the gradient. Even if both the gradient and flux are initially homogeneous, a small local steepening (flattening) of the gradient compared with its mean value results in a local turbulence response that further steepens (flattens) the gradient. The profile thus undergoes a kind of corrugation instability. Positive feedback provided by the instability is equivalent to a “negative diffusivity” that enhances the profile corrugation instead of smoothing, in contrast to conventional diffusion. The negative diffusion is often interpreted as the descending branch on an “S-curve” in the flux-gradient relation. Let us consider the ordinary Fick’s law, $\Gamma = -D(\nabla n)\nabla n$, and assume that the overall particle flux gradient dependence $\Gamma(\nabla n)$ flattens beyond the point when it decreases with $-\nabla n$ in a certain interval between $(-\nabla n)_1$ and $(-\nabla n)_2$. One may see then that the function $-\nabla n(\Gamma)$ has actually a shape of an “S-curve” on the $(-\nabla n, \Gamma)$ plane. Then the differential diffusivity, $\delta\Gamma/\delta(-\nabla n)$, becomes negative on one of the three branches of $-\nabla n(\Gamma)$ between $(-\nabla n)_1$ and $(\nabla n)_2$; see, e.g., Ref. [5]. This intermediate branch, however, constitutes the unstable state out of the three possible. The feedback loop, operating macroscopically, drives the transport supporting turbulence out of the regions with steep profiles $[-\nabla n > (-\nabla n)_2]$ into adjacent regions with flat ones $[-\nabla n < (-\nabla n)_1]$, so as to maintain the constant net flux Γ across the whole structure, which thus settles at a *bistable* equilibrium.

The staircase may be viewed as a *stationary* train of nonlinear pulses, much akin to those found in the FitzHugh-Nagumo system [6]. Each unit of the staircase consists of a jump, in which the system sits in the steep gradient root of the S-curve, and a step, in which it sits in the shallow gradient root. Transitions occur at corners, where entrainment and spreading are needed to ensure continuity of slopes. The theory for a single transport barrier is developed in Refs. [7,8]. A more general discussion may be found in Ref. [9].

Apparently, Philips [4] did not seek to present his mechanism as ubiquitous and universally applicable. However, the general principles behind it suggest looking for its applications to other media, where similar positive feedback may occur. For example, instead of negative diffusion, negative viscosity, also resulting from bistability, may generate strong flow shears. Furthermore, mixing of other quantities, such as temperature, PV, or salinity may also be considered. Dritschel and McIntyre [10] review and discuss the relation between the following three effects: mixing of PV, antifriction effects in horizontal stress, and spontaneous jet formation [11]. Balmforth *et al.* [12] elaborate on a mathematical model for staircase dynamics by evolving buoyancy and turbulent energy via two nonlinear diffusion equations, using a $k-\epsilon$ phenomenology while exploiting an amplitude- and scale-dependent mixing length. In a number of respects, our approach here is along the lines of Ref. [12], but because the model is different, so are the results. More about the relation of the present model to that developed in Ref. [12] can be found in companion papers [13,14].

Apart from fluid mechanics, a promising area for applications of the staircase concept is plasma transport in magnetic fusion devices, such as tokamaks. The idea of spontaneously formed transport barriers has attracted significant interest in the fusion community. A transport bifurcation in the fusion context was first observed in the ASDEX Tokamak [15]. This L \rightarrow H transition (from low- to high-confinement regime) occurred with the formation of a transport barrier at the tokamak edge, following a (local) transport bifurcation [16–22]. Although most of the research on tokamak transport barriers were concerned with such edge phenomena, interest in internal transport barriers is also significant [23–25]. Without much risk of oversimplification, a *staircase may be thought of as a quasiperiodic array of coupled internal transport barriers*.

Despite substantial differences in the mechanisms of transport bifurcation and transport barriers in fluids and plasmas, the apparent commonality of the phenomena suggests certain general principles behind transport barrier formation, their subsequent organization into staircases, and the prediction of their possible long-time evolution. We pursue these goals by using a simple generic staircase model, recently suggested. In the present paper, we report results on the following aspects of the staircase phenomenon. These include the following:

- (1) Identification of conditions and the parameter space for staircase formation.
- (2) The demonstration of staircase persistence by direct numerical integration of the model equations.
- (3) Finding exact analytic steady-state solutions, and exploiting these for code verification.
- (4) The elucidation of staircase dynamics, long-time evolution, merger events, and the role of domain boundaries. Special attention is focused upon the physics of mergers.

The plan of the remainder of the paper is as follows. In Sec. II we give a summary of the staircase model developed previously for geostrophic fluids and magnetized plasmas. Section III deals with the bistability conditions, boundary conditions, and parameter regimes required for the staircase formation. Section IV demonstrates staircase formation by direct numerical integration using the collocation BACOLI code developed in Ref. [26]. In Sec. V we present analytic steady-state solutions and use them to verify the numerical method. In Sec. VI the step coalescence (merger), long-time dynamics, quasiequilibrium staircase configuration, and accommodation of boundary conditions are discussed. Section VII presents discussion and conclusions.

II. STAIRCASE MODEL

The staircase model introduced previously, e.g., Ref. [13], and applied here to studies of formation and dynamics is relevant to both geostrophic fluids and magnetized plasmas. The model is one-dimensional (1D), which may appear deficient, but the staircase is a 1D structure by nature, so much can be learned about it from a 1D model. The gain for numerical calculations from such simplifications outweighs the limitations as it allows much longer integration with sufficient accuracy. As we will see, staircases typically exhibit disparate spatial scales and evolve at times very rapidly before they reach an asymptotic quasistationary regime. Moreover, after a long rest such a seemingly steady-state staircase may change abruptly by the merger of two adjacent steps into one in a matter of a tiny fraction of the rest time. These aspects of the staircase phenomenon make its studies computationally challenging, particularly regarding the proof of asymptotic robustness of these structures. So adaptive mesh refinement is clearly the method of choice in such studies [26]. Because of the disparate spatial and time scales discussed above, code verification is particularly important. A comprehensive code verification is possible in one dimension in time-asymptotic regimes by comparison with exact analytic solutions. Such solutions will be presented below.

The model that we use in this paper is described in detail previously, so we give only a short review. It is formulated in terms of the PV of a geostrophic fluid [27], such as the one on the surface of a rapidly rotating planet, i.e., the atmosphere or ocean. This (PV) quantity, q , consists of the planetary vorticity (which we take in the β -plane approximation) and fluid vorticity [2]:

$$q = \beta y + \Delta \Psi,$$

where Ψ is the stream function, and y is a latitudinal coordinate, which will remain after averaging over the longitude, x . By taking the curl of the Euler equation and adding a forcing term to its r.h.s. (which we specify later), one can derive the following equation for q :

$$\frac{\partial q}{\partial t} - \nabla \Psi \times \nabla q = \nu \Delta \Psi + f. \quad (1)$$

The vector product component perpendicular to the β plane is implied here. Next, we decompose q and Ψ into a mean and fluctuating part:

$$q = \langle q(y, t) \rangle + \tilde{q}(x, y, t)$$

with $\tilde{q} = \Delta \tilde{\Psi}$ and substitute this decomposition into Eq. (1). After separating the x -averaged component $Q \equiv \langle q \rangle$ from its fluctuating counterpart squared (enstrophy) $\varepsilon = \langle \tilde{q}^2 \rangle / 2$, a familiar closure problem of how to express $\langle \nabla \tilde{\Psi} \times \nabla \Delta \tilde{\Psi} \rangle$ through the averaged quantities ε and Q arises. For fluctuations which are statistically homogeneous in the x direction it is straightforward to obtain

the following (Taylor [28]) identity for the x -averaged PV flux Γ_q :

$$-\frac{\partial \Gamma_q}{\partial y} \equiv \langle \nabla \tilde{\Psi} \times \nabla \Delta \tilde{\Psi} \rangle = \frac{\partial^2}{\partial y^2} \left\langle \frac{\partial \tilde{\Psi}}{\partial x} \frac{\partial \tilde{\Psi}}{\partial y} \right\rangle.$$

The Taylor identity relates the PV flux to the Reynolds stress. Here we find it easier to work with PV than with momentum, as PV is locally conserved. By following the closure prescriptions discussed in previous papers, we apply a Fickian Ansatz for the PV flux: $\Gamma_q = -D_{\text{PV}} \partial Q / \partial y$, where $D_{\text{PV}}(\varepsilon, Q_y)$ is the PV diffusivity. Here and below we interchangeably use Q_y, Q_{yy} (and similarly for ε) for the respective y derivatives, $\partial Q / \partial y, \partial^2 Q / \partial y^2$. The PV diffusivity is assumed to follow a mixing-length hypothesis, $D_{\text{PV}} \sim l |\nabla \tilde{\Psi}|$, where $l(\varepsilon, Q_y)$ is the mixing length, introduced phenomenologically as

$$\frac{1}{l^2} = \frac{1}{l_0^2} + \frac{1}{l_R^2}. \quad (2)$$

Here l_0 is a fixed contribution to the mixing length l that characterizes the turbulence, e.g., the stirring scale, while l_R is the Rhines scale [29] at which dissipation of ε balances its production, so $l_R = l_R(\varepsilon, Q_y)$. The functional form of the diffusivity is $D_{\text{PV}} \sim (\varepsilon l^2)^{1/2} l$, where $l = l_{\text{mix}}$. The scale l_{mix} is chosen to be smaller of excitation scale l_0 and l_R the Rhines scale. The relaxation process studied in Ref. [30] also involved diffusive mixing of potential vorticity. However, there is no explicit appeal to minimum enstrophy theory. In turbulent cascades where the wave form of energy coexists with turbulent eddies the Rhines scale is where these two intersect, i.e., where $k\tilde{v} \sim \omega_k$ [29]. When the turbulent energy inverse cascade reaches this scale, it is intercepted and transported further by waves in both wave-number and configuration space. A macroscopic consequence of this includes structure formation. A somewhat related phenomenon is encountered in the context of ‘‘Alfvénization’’ of MHD cascades [31,32] in the solar wind and interstellar medium, where the ‘‘outer scale’’ energy is ultimately converted by waves into thermal and nonthermal plasma energy.

Note that the closure model presented here has a similar structure to that of direct statistical simulation (DSS). In particular, the potential enstrophy evolution equation balances growth, entrainment, and mean-field coupling with decay to small-scale dissipation with the forward cascade of enstrophy. Thus, this model goes beyond the pure ‘‘quasilinear’’ type of direct statistical simulation, to include some minimal representation for fluctuation damping by nonlinear transfer. More generally, both DSS and this closure account for mean field evolution and feedback. A variant of DSS and this closure account for forward cascade to dissipation. DSS focuses mainly on spectra, while this closure aims to elucidate real space structure. Indeed, there is a synergy between these two approaches.

Returning to Eq. (2), there is still considerable freedom in choosing the functional dependence of l_R on its arguments. The only dimensionless combination one may form using the variables entering Eq. (2) is $l_0^2 Q_y^2 / \varepsilon \equiv l_0^2 / l_R^2$. So we may slightly generalize the relation in Eq. (2) and write $l_0 / l = (1 + l_0^2 Q_y^2 / \varepsilon)^\kappa$. We choose $\kappa = 2$ and will comment on this choice in Sec. III. Replacing the eddy velocity in the Fick’s law by $l_0 \sqrt{\varepsilon}$ and measuring y in units of l_0 , we can write the averaged Eq. (1) as follows:

$$\frac{\partial Q}{\partial t} = \frac{\partial}{\partial y} \left[\frac{\varepsilon^{1/2}}{(1 + Q_y^2 / \varepsilon)^2} Q_y \right] + D \frac{\partial^2 Q}{\partial y^2}. \quad (3)$$

Here we added to the eddy diffusivity (the first term on the r.h.s.), a conventional collisional diffusivity D that may be associated with the molecular viscosity ν in Eq. (1). We prefer to consider it as a modest additive regularization of the turbulent diffusivity, $D_{\text{PV}}(\varepsilon, Q_y)$, discussed earlier. Applying similar argument to the turbulent part of PV and adding the terms responsible for its production, damping and unstable growth (see Refs. [13,14] for further details), we write an

evolution equation for the potential enstrophy ε as follows:

$$\frac{\partial \varepsilon}{\partial t} = \frac{\partial}{\partial y} \left[\frac{\varepsilon^{1/2}}{(1 + Q_y^2/\varepsilon)^2} \varepsilon_y \right] + D \frac{\partial^2 \varepsilon}{\partial y^2} + \frac{\varepsilon^{1/2}}{(1 + Q_y^2/\varepsilon)^2} Q_y^2 - \frac{\varepsilon^{3/2}}{\varepsilon_0} + \gamma \sqrt{\varepsilon}. \quad (4)$$

For the purposes of regularization, we use the same background diffusivity D as in Eq. (3) (see also below), γ is the strength of the forcing, while ε_0 quantifies the nonlinear damping of the enstrophy. Apart from these three parameters, the problem depends on the domain size in the y direction. Let us measure it in the units of l_0 and denote by L . Altogether, the system thus depends on four parameters (D , ε_0 , γ , and L), of which one can be removed by rescaling the variables. This reduction is, in fact, crucial to the search for staircase solutions, as they occupy a small domain in parameter space. So, by replacing

$$\varepsilon \rightarrow \gamma \varepsilon, \quad Q \rightarrow \sqrt{\gamma} L Q, \quad y \rightarrow Ly, \quad t \rightarrow \gamma^{-1/2} L^2 t, \quad (5)$$

Equations (3) and (4) transform to the following system:

$$\frac{\partial Q}{\partial t} = \frac{\partial}{\partial y} \left[\frac{\varepsilon^{1/2}}{(1 + Q_y^2/\varepsilon)^2} Q_y \right] + D \frac{\partial^2 Q}{\partial y^2}, \quad (6)$$

$$\frac{\partial \varepsilon}{\partial t} = \frac{\partial}{\partial y} \left[\frac{\varepsilon^{1/2}}{(1 + Q_y^2/\varepsilon)^2} \varepsilon_y \right] + D \frac{\partial^2 \varepsilon}{\partial y^2} + L^2 \left\{ \frac{Q_y^2}{(1 + Q_y^2/\varepsilon)^2} - \frac{\varepsilon}{\varepsilon_0} + 1 \right\} \varepsilon^{1/2}, \quad (7)$$

and the integration domain is now $y \in [0, 1]$. These are strongly nonlinear driven or damped parabolic equations possessing numerous stationary and time-dependent solutions. In the next section, we discuss the strategy of our search for the solutions with required staircase properties. To conclude this section, we consider the total enstrophy budget by introducing this quantity as

$$\mathcal{E} \equiv \int_0^1 (Q^2/2 + \varepsilon/L^2) dy.$$

From Eqs. (6) and (7), we obtain

$$\frac{d}{dt} \mathcal{E} = \int_0^1 \sqrt{\varepsilon} \left(1 - \frac{\varepsilon}{\varepsilon_0} \right) dy + \frac{\sqrt{\varepsilon} (\varepsilon_y/L^2 + Q Q_y)}{(1 + Q_y^2/\varepsilon)^2} \Big|_0^1 - D \left(\int_0^1 Q_y^2 dy + Q Q_y \Big|_0^1 \right).$$

It is seen that the volumetric enstrophy production due to the instability (first term under the first integral) can be balanced by the nonlinear damping (second term under the integral). The possible enstrophy leak through the boundaries (second term) and small diffusive dissipation can also be compensated by adjusting the nonlinear dissipation rate, $\propto \varepsilon_0^{-1}$.

III. STAIRCASE PREREQUISITES

A numerical integration of Eqs. (6) and (7), if not thoroughly planned, shows that staircases (SCs) are not ubiquitous solutions that arise from almost any randomly chosen set of parameters and initial conditions. On the contrary, one needs to search for them carefully in a multidimensional parameter space. However, as we will see from the sequel, once the appropriate corner in the parameter space is located, the SC solutions arise as remarkably robust asymptotic attractors of the system given by Eqs. (6) and (7). Apart from the three parameters directly entering these equations (D , L , ε_0), two or three additional parameters enter from the boundary conditions for Q and ε , depending on assumptions, discussed briefly below.

First, throughout this paper we impose Dirichlet boundary conditions but fix a PV contrast across the domain, thus maintaining a constant average flux. Specifically, we assume a SC structure to form in a limited y domain (in our variables $y \in [0, 1]$). On each side of this domain a stationary level of

ε is maintained, which in most of the cases considered in this paper is the same: $\varepsilon(0, 1) = \varepsilon_B$. This reduces the total number of parameters by one. Next, the PV, Q , is determined up to an arbitrary constant, so we fix its value on one end, $Q(0) = 0$. Then we set $Q(1) = Q_B$, so the enstrophy inside the staircase is driven by the gradient Q_y [the first term in braces in Eq. (7), with $\langle Q_y \rangle = Q_B$], in addition to the constant drive given by the very last term in the braces. At a minimum, we thus have a 5D parameters space to search in for a SC solution. Clearly, we need directions for our search.

In rough terms, a SC structure described in Sec. I may result from the loss of stability of a ground-state solution of Eqs. (6) and (7) characterized by the constant values $\varepsilon = \varepsilon_B$ and $Q_y = Q_B$ that annihilate the term in braces in Eq. (7). Then nonlinear saturation of the instability may possibly lead to a (quasi)stationary SC solution. A generic paradigm here is *bistability, where apart from the unstable ground state, there exist two stable steady states*. The system jumps to one of these when the ground state becomes unstable. To explain the conditions for this scenario, let us denote the enstrophy production-dissipation term in braces on the r.h.s. of Eq. (7) as

$$R \equiv \frac{Q_y^2}{(1 + Q_y^2/\varepsilon)^2} - \frac{\varepsilon}{\varepsilon_0} + 1. \quad (8)$$

A staircase, particularly the one with a large number of steps, evidently requires $L \gg 1$. Otherwise, the diffusive terms in Eqs. (6) and (7) will dominate, thus driving the ε and Q_y profiles to constants. Therefore, assuming $\partial_t Q \approx 0$ and $L \rightarrow \infty$, it follows that $R \rightarrow 0$. Thus, with some reservations discussed below, Eq. (7) can be written for $L \gg 1$ as

$$\varepsilon_t = L^2 \sqrt{\varepsilon} R(\varepsilon, Q_y). \quad (9)$$

It should be noted here that (as $L \gg 1$) the first two terms on the r.h.s. of Eq. (7) are small terms, with higher derivative discarded in Eq. (9). Boundary layers are expected between the states with high and low values of ε associated with two stable fixed points in Eq. (9). Also note that Q_y may (and will) jump between these fixed points along with ε , but the jump description requires treating the neglected higher derivative terms that will be taken into account in Sec. V. We will call the thin regions over which ε and Q_y jump the ‘‘corners,’’ as they appear as such in the $Q(y)$ profile (see Fig. 4 below). A region of flat Q (large ε) attached to the corner on one side we call a ‘‘step.’’ A contrasting region, where Q is steep (small ε), we call a ‘‘shear layer’’ or ‘‘jump.’’ In essence, such structure corresponds well to the SC phenomenon, since the corners between the shear layers and steps, as envisioned by Phillips [4], are simply the internal boundary layers.

The conditions for generating the SC structures described above can be approached assuming constant local enstrophy and vorticity gradient ε , $Q_y \equiv \text{const}$. Here we constrain the parameters in the driving term R to have a bistable form shown in Fig. 1. In this case, the alternating layers correspond to jumps between two stable equilibria (fixed points) over an unstable one. Of course, one can directly solve the cubic relation $R = 0$ for, e.g., ε as a function of Q_y and ε_0 , thus determining conditions for the three roots to exist. However, this approach is algebraically tedious, so we take a different route. First, denote $\xi \equiv \varepsilon/Q_y^2 = l_R^2$ and rewrite the equation $R = 0$ after dividing it by Q_y^2 :

$$F(\xi) \equiv \frac{\xi}{\varepsilon_0} - \frac{\xi^2}{(1 + \xi)^2} = \frac{1}{Q_y^2}. \quad (10)$$

In this form, the variables ξ and Q_y are separated while ε_0 is considered as a constant parameter. For this equation to have three real roots (the scenario of bistability), the value $1/Q_y^2$ must fall between the local extrema of $F(\xi)$, provided that they exist:

$$F_{\min} < Q_y^{-2} < F_{\max}$$

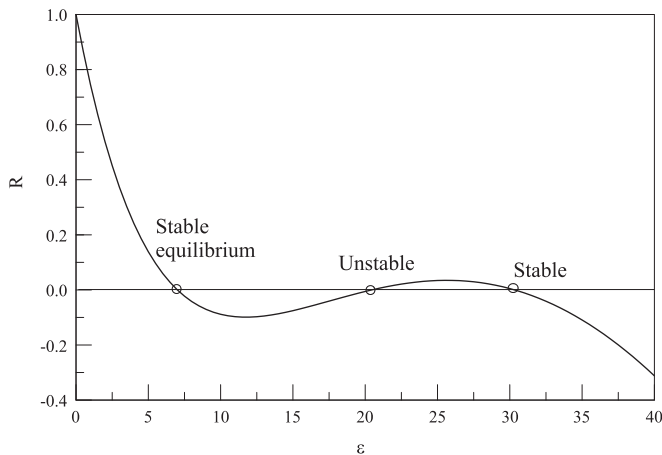


FIG. 1. Entrophy production-dissipation term R in Eqs. (7) and (8) as a function of entrophy ε , shown for a fixed mean vorticity gradient $Q_y = 35$ and $\varepsilon_0 = 3.55$.

(see Fig. 2). Denoting the points of extrema by $\xi_{0,1}$, this constraint can be written, using Eq. (10) as follows:

$$\xi_1(1 - \xi_1) < \frac{2\varepsilon_0}{Q_y^2} < \xi_0(1 - \xi_0). \quad (11)$$

Note that the left term of this inequality becomes negative for sufficiently large ε_0 (lower curve in Fig. 2). The two extremal points of $F(\xi)$, $\xi_0 < \xi_1$, where $F'(\xi_{0,1}) = 0$, are also to be found from a cubic equation, but this equation is much simpler than the original one, given by Eq. (10). The requirement for the two isolated roots $\xi_{0,1}$ to exist is $\varepsilon_0 > 27/8$ (Appendix A). This condition proved very useful in the search for a SC regime. However, the latter is not precise in that Q_y and ξ also change during the transition from one stable state to the other. In fact, one can easily determine $Q_y(\xi)$ variation by assuming that it changes in space but remains stationary. This assumption relates Q_y to ξ by the constant diffusive flux in Eq. (6). Denoting the flux of Q by b (see Appendix A and Eq. [13] below) we obtain the following relation for Q_y to be used in the constraint (11) for

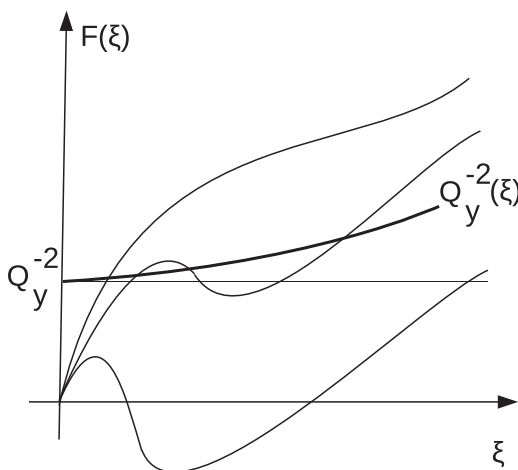


FIG. 2. Left-hand side of Eq. (10), $F(\xi)$, schematically drawn for three different values of parameter ε_0 .

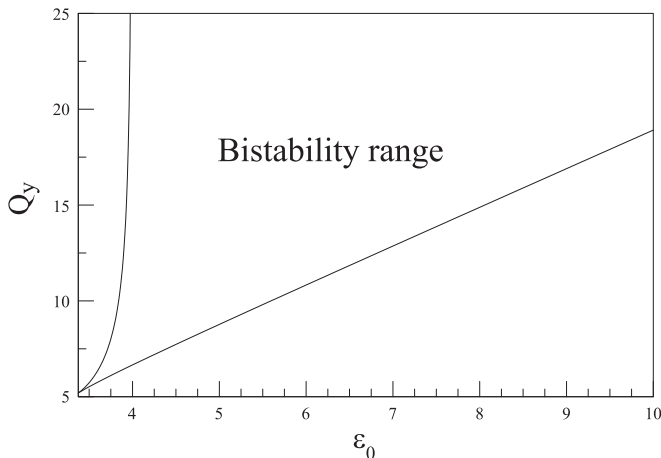


FIG. 3. Part of parameter space in variables ε_0, Q_y where the SC solutions are possible.

connecting the two stable roots of Eq. (10):

$$\frac{1}{Q_y} = \frac{D}{2b} + \sqrt{\frac{D^2}{4b^2} + \frac{\xi^{5/2}}{b(1+\xi)^2}}. \quad (12)$$

By substituting the last relation into the r.h.s. of Eq. (10), one can solve it for ξ in terms of the three parameters ε_0, D , and b . For certain values of these parameters, three isolated roots are possible, of which the largest and the smallest correspond to neighboring layers in a SC solution, or to the two stable roots of the truncated equation (9). The intermediate root is unstable. For practical reasons, instead of locating all three roots, we constrain the parameter space by the simple analytic formulas (11) and (A1). They provide a range of Q_y for possible SC solutions in terms of ε_0 . The region in the ε_0, Q_y plane in which to look for the staircase numerically is shown in Fig. 3.

It follows that a stationary SC structure is a quasiperiodic sequence of regions with alternating upper and lower stable ε values in Fig. 1. As we will see in the sequel, time-asymptotically this solution can be calculated analytically. The exact analytic solution provides both a guidance in exploring the time-dependent regimes and an excellent code verification tool.

In addition to the above guidance, the following consideration has proven useful in search for SC solutions. As they result from an unstable stationary solution with initially constant ε and Q_y , a stability analysis of the full system can be performed. This replaces the local analysis above, based on the zeros of the function $R(\varepsilon)$ and signs of its derivatives $R'(\varepsilon)$. This extended analysis, even if it probes only simple perturbations of the type $\propto \exp(iky - i\omega t)$, is rather tedious. It is also more restrictive, as it does not capture the bistable state described earlier. So we do not reproduce the linear analysis here. However, a broader insight into the parameter choice for obtaining the SC solution has been gained from this analysis. As mentioned earlier, the mixing length scaling in Eq. (2) can be written more generally as $l_0^2/l^2 = (1 + l_0^2/l_R^2)^\kappa$, and the stability analysis can be performed for this, more general form of the mixing length. Our particular choice $\kappa = 2$ in the model equations (6) and (7) was precisely dictated by the instability condition for a steady-state solution with constant ε and Q_y . At the same time, even without performing such a stability analysis of the full system, an alternative choice $\kappa = 1$ instead of $\kappa = 2$ may be shown to be inconsistent with SC solutions; namely, the denominator of the first term in R from Eq. (8) is simply $1 + Q_y^2/\varepsilon$ in this case. Therefore, the function $R(\varepsilon)$ has only one positive stable root at which $R'(\varepsilon) < 0$. Hence, no bistability occurs, so no staircase forms!

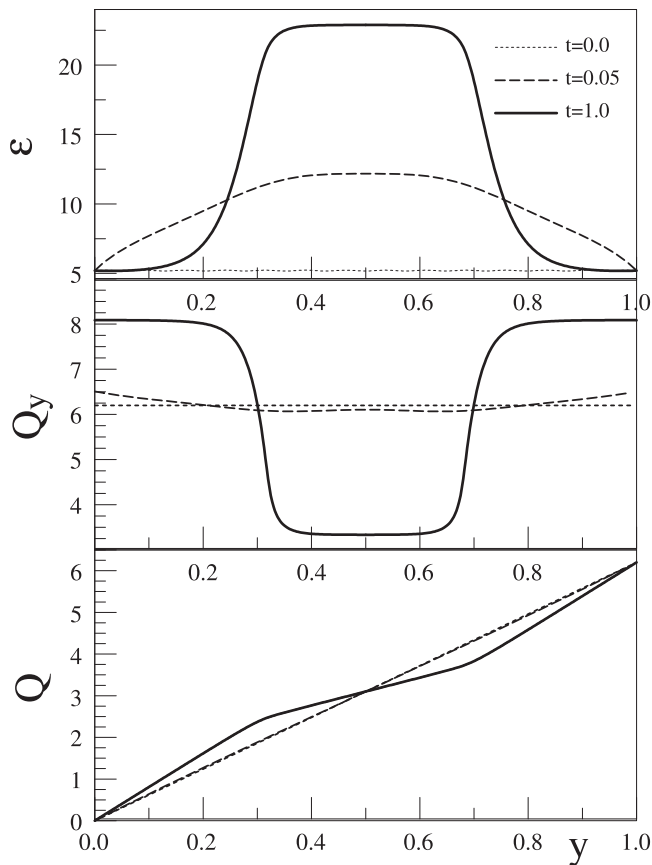


FIG. 4. Generation of a one-step profile out of an unstable ground state superposed by small perturbations (short-dash lines). Perturbations are low-amplitude, so short scales are not seen clearly in the initial profile but they do not affect the profile evolution significantly. The Dirichlet boundary conditions are applied for Q and ε at both boundaries. The other parameters are $\varepsilon_0 = 3.8$, $L^2 = 2.3 \times 10^3$, $D = 1.5$; the boundary conditions can be read from the plots.

Another important aspect of the stability analysis regards the possible number of steps in the structure. Indeed, by contrast to the above discussed *local* bistability based on Eq. (9) (in essence, a $k \rightarrow 0$ limit), the standard linear analysis assumes perturbations of the form $\propto \exp(-i\omega t +iky)$. The small scales are damped, as $\Im\omega \simeq -k^2$, but the growth rate turns positive for small k and sufficiently large L . Thus, there must be a maximum unstable k , and possibly even maximum $\Im\omega(k)$, depending on the boundary conditions. *This k sets the number of steps in the staircase!* However, as numerical integration shows, *this initial number* (being also somewhat sensitive to the initial conditions) *quickly relaxes to a smaller number of steps, as the staircase grows to a nonlinear level.* This quasiequilibrium SC configuration and its time evolution are the main focus of our study below.

IV. STAIRCASE FORMATION

It follows from the above considerations that the number of steps in a staircase must grow with the parameter L . It is thus natural to assume that at some moderate value of L , this number can be as small as one. Shown in Fig. 4 is a one-step profile generated from an unstable ground state with

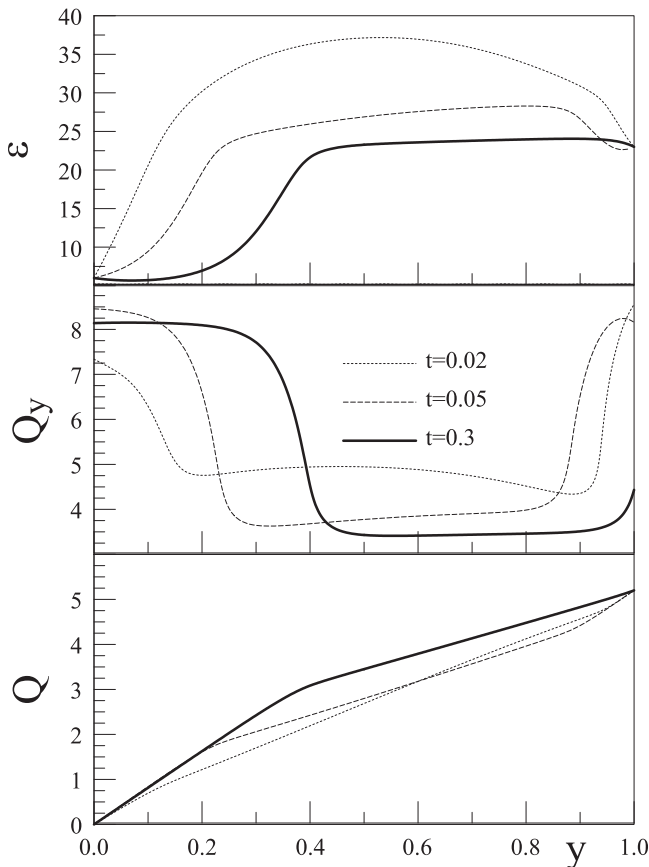


FIG. 5. The same plots as in Fig. 4 but for $L^2 = 900$. The other parameters are the same, except the turbulence level is kept at different levels on the right and left boundary (6.0 and 23.0, respectively). Initially, it is a linear function superposed by a sinusoidal with a short scale (~ 0.03) and small amplitude (≈ 0.03). Since parameter L is relatively small, the short-scale initial perturbations do not grow (cf. Fig. 10 below). As the midplane symmetry is broken, the initially formed profiles propagate to the right boundary. After $t \lesssim 1$, the Q -profile relaxes to one step at the right boundary and a shear layer at the left. This configuration persists in time, as the boundary conditions are consistent with a part of periodic stationary solution (Sec. V) that fits into the integration domain.

small-scale weak perturbations (short-dash lines) superposed. The initially small scales are quickly damped, and the system evolves to a one-step profile, shown by heavy lines. In Sec. V we will demonstrate that this profile coincides with an exact stationary solution of the system. As it appears to be stable, it must persist indefinitely, thus constituting a single-step attractor. The ε and Q_y profiles are symmetric with respect to the midplane, as the boundary conditions also are $\varepsilon(0) = \varepsilon(1)$.

An example of asymmetric profile is shown in Fig. 5. In this case, the boundary conditions are different at the left and right boundary, $\varepsilon(0) \neq \varepsilon(1)$. Although the system also evolves into a staircase with only one step, this time the step attaches itself to one of the boundaries. The steep part of the Q -profile attaches itself to the opposite boundary.

Now that we have demonstrated that a stationary staircase is indeed a strong attractor for the time-dependent system given by Eqs. (6) and (7), it is worthwhile to investigate all possible steady-state solutions analytically. This investigation will be useful in numerical studies of SC dynamics, presented later in Sec. VI.

V. ANALYTIC SOLUTION FOR TIME-ASYMPTOTIC STAIRCASE

Analytical time-asymptotic SC solutions can be obtained easily. These solutions are also relevant to the SC dynamics since, as we will see from the numerical studies, a typical multistep staircase does not change in time, apart from quick merger events. One may refer to it as “metastationary.” Between such merger events, the staircase is perfectly described by analytic solutions that we obtain below and compare against numerical solutions in Sec. V A.

Assuming a steady state, from Eq. (6) we deduce

$$\left[\frac{\varepsilon^{1/2}}{(1 + Q_y^2/\varepsilon)^2} + D \right] Q_y \equiv b = \text{const.} \quad (13)$$

Instead of Q and y , it is convenient to use the following two variables as dependent and independent, respectively:

$$\psi = \frac{Q_y}{\sqrt{\varepsilon}}, \quad \eta = \sqrt{2L}y, \quad (14)$$

We keep ε as the second dependent variable. Assuming also $\partial\varepsilon/\partial t = 0$, multiplying Eq. (7) by a factor $2\varepsilon_y/bQ_y$ and integrating once in y , we arrive at the following first integral of the equation

$$\frac{\varepsilon_\psi^2}{\psi^2\varepsilon} \left(\frac{d\psi}{d\eta} \right)^2 + W(\psi) = E = \text{const.}, \quad (15)$$

where $\varepsilon_\psi = \partial\varepsilon/\partial\psi$ and

$$W(\psi) = \varepsilon - \frac{2D}{3b}\psi\varepsilon^{3/2} + \frac{\varepsilon}{b\psi} \left(1 - \frac{\varepsilon}{2\varepsilon_0} \right) + \frac{2D}{3b} \int \varepsilon d\psi + \frac{1}{b} \int \frac{\varepsilon}{\psi^2} \left(1 - \frac{\varepsilon}{2\varepsilon_0} \right) d\psi. \quad (16)$$

Using Eqs. (13) and (14), $\varepsilon(\psi)$ can now be written in the following explicit form:

$$\varepsilon = (1 + \psi^2)^2 \left[\sqrt{\frac{b}{\psi} + \frac{1}{4}D^2(1 + \psi^2)^2} - \frac{1}{2}D(1 + \psi^2) \right]^2. \quad (17)$$

It follows that the first integral in Eq. (15) provides the steady-state solution of Eq. (7) in the form of $\psi(\eta)$, which can be obtained by inverting the function $\eta(\psi)$. This in turn, can be derived from Eq. (15) by quadrature. Furthermore, using Eqs. (14) and (17), one can obtain the steady-state solution in original variables, $Q(y)$ and $\varepsilon(y)$.

For the purpose of comparison of the solution given by Eq. (15) with the asymptotic regime obtained from the numerical integration of Eqs. (6) and (7), we return to the original coordinate y and write the solution in the form of $y = y(\psi)$:

$$y = \frac{1}{\sqrt{2L}} \int \frac{\partial\varepsilon}{\partial\psi} \frac{d\psi}{\psi \sqrt{\varepsilon[E - W(\psi)]}}. \quad (18)$$

Apart from an arbitrary constant y_0 , that can always be added to the r.h.s. to adjust the position of the staircase in y , the solution $\psi(y)$ in Eq. (18) depends on two further constants, E and b . The latter is the flux of Q that enters W in the last expression by virtue of Eq. (16). Although b is related to the boundary conditions because of Eq. (13), under the Dirichlet boundary conditions employed here Q_y is not fixed at the boundaries. Therefore, b becomes constant only when the system reaches a steady (or metastationary, as discussed earlier) state. Before such a state, presented in Eq. (18), is reached b changes in time. The role of the constants E and b can be elucidated by returning to the first integral in Eq. (15) and interpreting it as a constant total energy of a pendulum with a variable mass [coefficient in front of $(\partial\psi/\partial\eta)^2$] moving in a potential well $W(\psi)$. The variable ψ plays the role of a coordinate here while η is “time.” One form of $W(\psi)$, shown in Fig. 6, corresponds to a specific value of $b = b_*$ for which the two maxima of $W(\psi)$ are equal. This is an important case

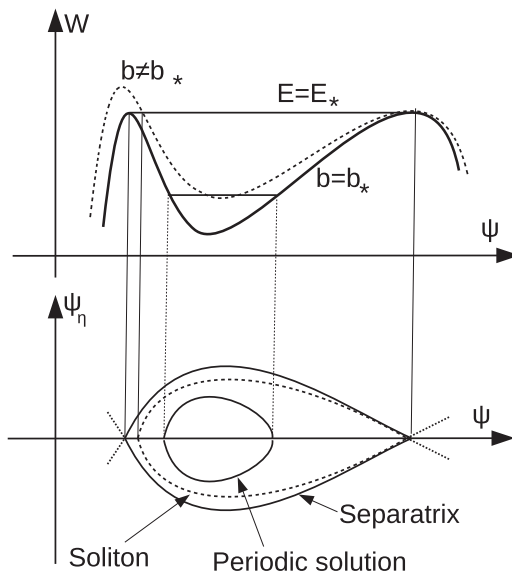


FIG. 6. “Oscillator’s” pseudopotential and its phase plane. The top panel shows the function $W(\psi, b)$ from Eq. (15) for the case when two maxima that correspond to two zeros of function $R(\varepsilon)$ in Eq. (8) are at the same value of $W = E_{\max}$. The maxima are the same for a specific value of the constant flux b in Eq. (6). For $E < E_{\max}$ solutions are periodic.

since it admits heteroclinic orbits connecting two hyperbolic points of the “pendulum” at a specific value of $E = E_*$. The orbits correspond to the two branches of a separatrix shown on the phase plane in Fig. 6. These particular values of $b = b_*$ and $E = E_*$ correspond to an isolated transition from low to high values of ψ , when y runs from $-\infty$ to $+\infty$. The original variables ε and Q_y can always be restored unambiguously from $\psi(y)$ using Eqs. (17) and (14). The mirror branch of this orbit corresponds to the reverse transition, and fixed points correspond to the two stable roots of the function $R(\varepsilon)$ introduced in Sec. III and depicted in Fig. 1. Clearly, for a heteroclinic orbit to exist the two areas cut by the abscissa from $R(\varepsilon)$ curve between the stable and two unstable roots must satisfy a certain relation. This is that measured (integrated) in the variable y instead of ε , and these areas must be equal, as it follows from the derivation of Eq. (15). Using the pendulum analogy again, the heteroclinic orbit connects two unstable equilibria (the two humps on the potential energy profile). Therefore, the accelerating phase of the trajectory must be exactly annihilated by the decelerating phase. This is equivalent to the familiar Maxwell’s construction, illustrated in Fig. 7. The Maxwell rule is common for other transition phenomena, both flux and source driven [6–8]. For values of parameters E and b other than discussed above, the solutions given by Eq. (18) fall in two further categories: (1) strictly periodic solutions corresponding to $E < E_*$, while b may or may not remain equal to b_* (Fig. 6), and (2) soliton-type solutions when the orbit is homoclinic, starting and ending at one of the two hyperbolic points. Here $b \neq b_*$, $E = E_*$, so we have only one hyperbolic fixed point on the orbit. Just as the heteroclinic solution described earlier, this solution also becomes periodic for $E < E_*$. The periods of solutions with $E < E_*$ can be calculated using Eq. (18) as

$$\mathcal{L}(E, b) = \frac{\sqrt{2}}{L} \int_{\psi_1}^{\psi_2} \frac{\partial \varepsilon}{\partial \psi} \frac{d\psi}{\psi \sqrt{\varepsilon[E - W(\psi)]}}. \quad (19)$$

Here the integral runs between the two turning points obtained from the relation $W(\psi) = E$. By contrast with compact solutions, i.e., isolated transitions or solitons (which do not “fit” into a finite domain), the periodic solutions can be fully described on a $[0, 1]$ segment, provided that $\mathcal{L} < 1$. In

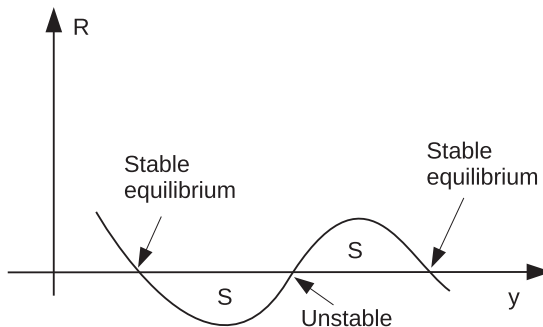


FIG. 7. Illustration of a Maxwell transition rule, in a form of the production-dissipation function, $R(y)$. In order to connect the two stable equilibria, shown in Fig. 1, with one heteroclinic orbit, shown in Fig. 6, the areas above and below the abscissa must be equal.

general, however, and especially when $n\mathcal{L} \neq 1$ with $n = 1, 2, \dots$, the boundary conditions need to be consistent with parameters b and E . We will touch upon this aspect of the solution later.

A. Comparison of time-asymptotic numerical solutions with the analysis

A comparison of the analytic solutions given above with those obtained numerically serves several purposes. First, it verifies the code's accuracy and convergence, while establishing its limitations. The latter is particularly important in view of the time- and space-scale disparities inherent in this problem. Second, it verifies that the analytic solutions are indeed the attractors for the time-dependent solutions. In addition, the numerical integration delineates the basins of attraction of these analytic solutions. Finally, such comparison gives insight about a possible evolution of the system beyond the accessible integration time. The latter aspect is crucial in that the time-dependent solutions typically show a long rest-transition burst alternation. Figure 8 shows an example of such behavior. After quick ($t \lesssim 0.1$) mergers of the 10 out of the 12 initially formed steps ($10 \rightarrow 5$),

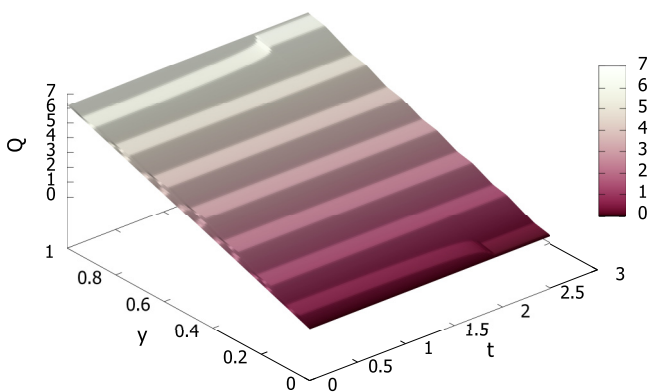


FIG. 8. Merger of steps shown as a surface plot of the mean vorticity $Q(t, x)$ with the Dirichlet boundary conditions, $\Delta Q = 6.2$, between the right and left boundary, $\varepsilon_0 = 10.38$, $L^2 = 1.5 \times 10^5$, $D = 1.7$. Initially, as many as 12 steps are formed, but very rapidly ($t \lesssim 0.1$) they merge to 7. The seven-step configuration lasts with no numerically significant changes up to the moment $t \approx 2$ when two shear layers near the walls disappear and the edge steps merge into respective walls. The remaining SC structure persists up to $t \approx 100$ when the two edge steps merge with their neighbors.

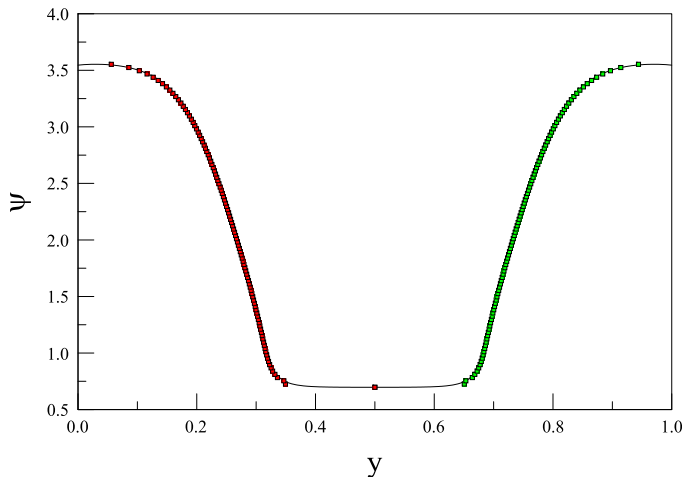


FIG. 9. Numerical solution of Eqs. (6) and (7) in long-time asymptotic regime, shown with the solid line. The parameters are the same as in Fig. 4. Exact analytic solution represented by the two branches of $y(\psi)$ in Eq. (18), shown with red and green squares. The insignificant deviations at the top and the bottom of the curve are due to the limited accuracy of numerical integration at the end points in Eq. (18).

the systems sits at the state of seven remaining steps for a long time, $t \approx 2$. Moreover, at this time the staircase merely accommodates the boundary conditions by attaching each of the two edge steps to the respective boundary, Fig. 8. In the next section, a case of much longer rest will be presented. We will also take a closer look at a typical merger event. Without analytic predictions, it is difficult, if not impossible, to tell whether the long rests are genuine attractors of the system or the next merger is to be expected. If it is, then what determines the waiting time? Conversely, if a merger occurs after a long rest period—during which the profile agrees with one of the stationary analytic solutions—one may consider such a merger as a spurious effect of accumulated round-off errors. For the purpose of comparison with numerical solutions, the constants b and E —which an analytic solution depends upon—should be calculated using boundary conditions imposed on the numerical solutions. More practically and equivalently, we extract them directly from the numerical solution already shown in Fig. 4. An exact analytic solution, plotted using Eq. (18), is compared to this numerical solution in Fig. 9. Given the parameters b and E , the analytic solution is obtained by a simple tabulation of the integral in Eq. (18), even without regularization of the integrand singularities at $W = E$. This explains a nonuniform, coarse sampling, as well as a minor deviation of one point next to the minimum of $\psi(y)$ from the numerical curve. The extrema of $\psi(y)$ obviously correspond to the algebraic ($E < E_*$) or logarithmic ($E = E_*$) singularities of $y(\psi)$.

The parameters and boundary conditions for the run in Fig. 9 are such that the entire profile spans slightly more than one period of the respective analytic solution, $\mathcal{L} \lesssim 1$. Furthermore, in the asymptotic state shown in the figure, the flux b is constant throughout the integration domain to within the code accuracy, so the solution is indeed steady. Note that we varied the code error tolerance between 10^{-8} – 10^{-6} (see Ref. [26] for the algorithm’s description and further references) without sizable effects on convergence, up to $t \sim 100$. Further details on the comparison of analytical and numerical solutions are given in Appendix B.

These results, and particularly the perfect agreement between the overall analytic and numerical solutions along with the code convergence (insensitivity to the error tolerance), increase our confidence that the code accurately describes the evolution of the SC system in time.

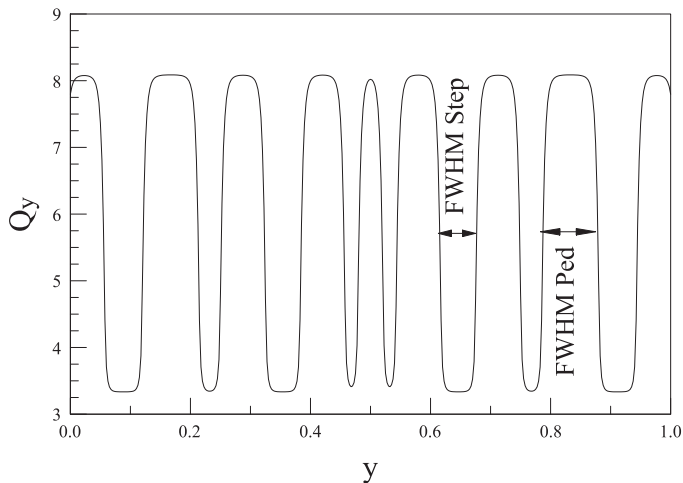


FIG. 10. Typical profile of Q_y , where FWHM (full width at half maximum) characterizes the width of shear layers (“humps” on Q_y or “pedestals” on the Q -profile) and steps (troughs) on the plot. Here $D = 1.5$, $L^2 = 10^5$, $\varepsilon_0 = 3.7915$, $Q(1) = 6.2$, and $\varepsilon(0, 1) = 10.38$.

VI. STAIRCASE MERGER EVENTS

The purpose of this section is to connect SC mergers with the analytic properties discussed in the previous section. Within the range of parameters outlined in Sec. III, the numerical integration of Eqs. (6) and (7) consistently demonstrates the following evolution: long metastationary periods interspersed by quick SC mergers. During these periods, the SC configuration does not change in any noticeable way and is accurately described by analytic solutions obtained in the preceding section. Natural questions then are: what causes the next merger, and does it become final—beyond which the SC configuration will stay unchanged. Here the word “unchanged” should be taken with caution, as our simulations clearly show that nearly perfectly stationary SC configurations lasting for $t \gtrsim 100$ do merge eventually, and over times $t \lesssim 0.1$. Recall that time here is given in units of $L^2/\sqrt{\gamma}$, Eqs. (4) and (5). Despite these remarkably disparate timescales, the answer that we find below is at least consistent with the analytic solutions. Typically, a quasistationary staircase forms very quickly ($t \ll 1$) with n steps separated by shear layers exhibiting a significantly steeper gradient of the mean vorticity Q_y also with suppressed enstrophy level, ε . The number n is determined by the maximum growth rate (similarly to the results of Ref. [12]; see also Sec. III) and partly by the initial conditions. Then, over a somewhat longer time (but still $t < 0.1$), most—except the boundary-attached—steps merge with their neighbors. So the total number of steps becomes $\approx n/2$. This phase of the SC evolution is illustrated in Fig. 10, whose time history will be illustrated in Fig. 11. After this initial phase the staircase persists for a much longer time. It is clear from the surface plot of the Q -flux that it grows rapidly and deviates strongly from its globally constant value precisely at the merger locations.

The further fate of a quasistationary staircase depends on the following factors. One factor is the proximity of the staircase to the periodic solution described in Sec. V. The portions of the SC profile that are periodic do not merge, consistent with the analytic solutions. As we have seen, all stationary solutions are exhausted by either periodic or compact (solitary- or kink-type) solutions [33]. Therefore, the periodic segments of the staircase tend to be steady. An example of such a staircase is shown in Fig. 8. After quick initial mergers, this staircase remains periodic in its interior, and only the edge regions deviate from spatial periodicity. Here the second factor that influences the evolution of a staircase enters. This is the boundary effect. Indeed, as we discussed in Sec. VA, at $t \approx 2$ the edge shear layers disappear, and the edge steps attach themselves to the boundaries. An

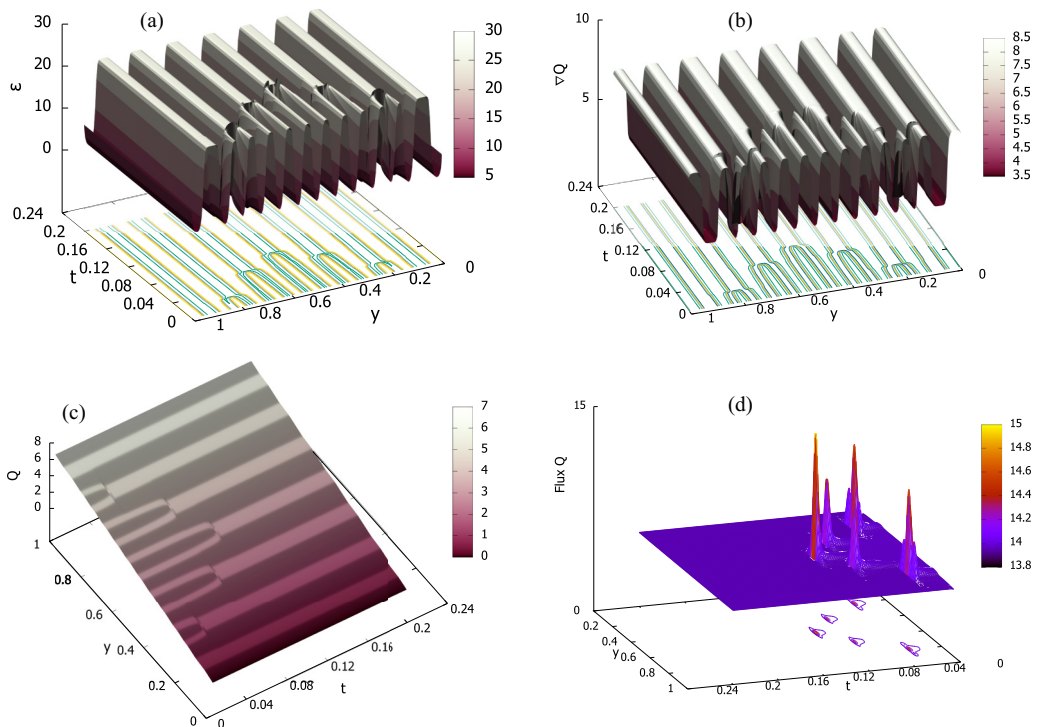


FIG. 11. Time history and details of the SC merger sequence that led to the profile shown in Fig. 10. Panels (a) and (b) show the enstrophy ε and Q_y , while panels (c) and (d) show the mean potential vorticity Q and its flux given by Eq. (13). The early relaxation phase $t \lesssim 0.01$ is removed from the plots to emphasize the flux strong variation during the later SC mergers. Abrupt drops in the Q -flux excess at the merger sites after initially slow and then explosive growth are clearly seen in panel (d). It is also notable from, e.g., panel (a) that a merger still produces some small effect on the nearest seemingly unaffected steps.

inspection of the Q -flux shows that it remains constant in the interior where the staircase is periodic, and it progressively deviates from the constant values near the boundaries. This ultimately results in the boundary accommodation event at $t \approx 2$, after which the flux returns to its global average. After this event, however, the staircase becomes nonperiodic at the edges (edge steps are broader than the central ones). As expected, the edge steps merge with their neighbors, but only at $t \approx 100$.

A different example of a staircase, which is noticeably *nonperiodic*, is shown in Fig. 10. Such configurations tend to merge over significantly shorter time, particularly at those locations where the steps or shear layers are close to each other. So the spacing between the neighboring corners is important for the mergers. These corners separate steps from shear layers. As we know, a single corner with a step and a shear layer on each side makes a stationary structure in an infinite space and is described by a heteroclinic orbit. It approaches exponentially constant values at $\pm\infty$ that characterize the step and the shear layer, respectively. Two neighboring corners, for example, form either an isolated step or isolated shear layer (e.g., Fig. 4). Based on Sec. V, this construction does not belong to any type of stationary solution in infinite space. However, if its corners are well separated by a broad step or shear layer, their interaction term is $\sim \exp(-L\Delta y) \ll 1$, where Δy is the distance between the corners and $L \gg 1$ (see Sec. V and Fig. 4). So, broad, well-separated steps and layers in a staircase must also persist in time. Typically, when the system relaxes to four or five, not perfectly periodic steps, the next merger occurs after several hundreds of time units. Integration beyond this time would require a significantly lower error tolerance. Under these circumstances, analytic predictions become much more reliable than numerical ones.

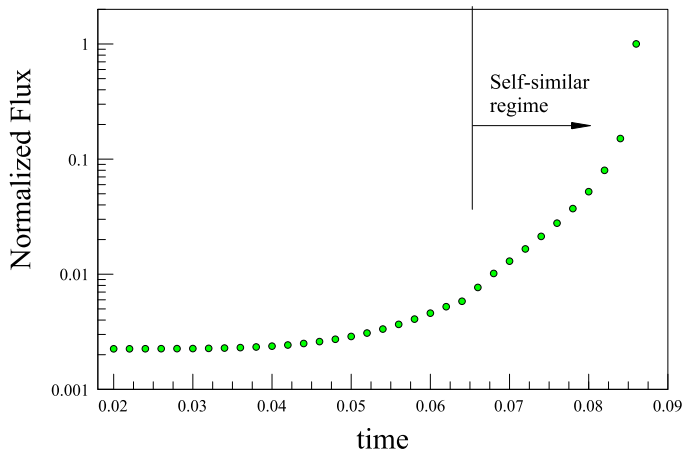


FIG. 12. Q -flux as a function of time immediately before and during the merger event near $t \approx 0.09$ at the middle of integration domain at $y = 0.5$ shown in Fig. 11. For the clarity of representation and a functional fit, shown in Fig. 13, the flux is adjusted by subtracting a reference value $F_B \approx 13.96088$, which is close to a globally averaged flux.

SC steps merge in a rather interesting way. Figure 11 shows a sequence of such mergers of 12 initial steps (see the Q -panel). The mergers proceed symmetrically from the boundaries towards the center of the integration domain. This process continues until the mergers converge at the center and the central two steps merge into a bigger step. Here we concentrate on this last merger by zooming into it in time. The best variable for characterization of the merger is the Q -flux, which is shown in Fig. 12 at the point $y = 0.5$ as a function of time. The flux remains constant when no mergers occur (constant b in stationary solutions of Sec. V), so we subtract this constant value for clarity and for the purpose of functional fitting below. As seen from the plot, the flux builds up in two distinct phases before it drops abruptly to its averaged value after the merger. The first phase is an initial growth that lasts to about $t \approx 0.065$. The flux increase remains relatively small, $\lesssim 0.01$. The second

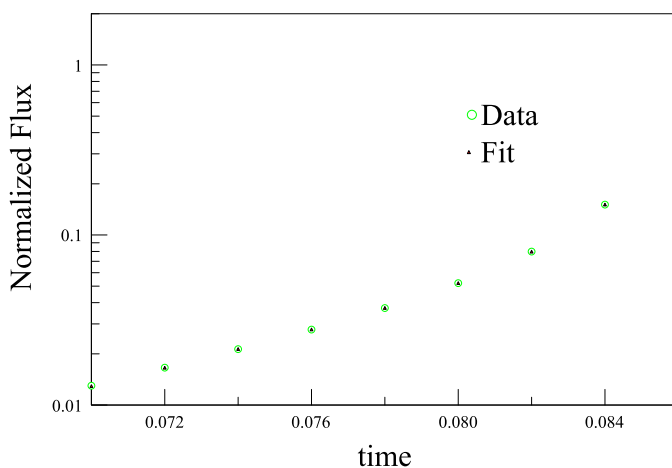


FIG. 13. Fit of the flux in its self-similar phase of evolution for $0.070 < t < 0.086$. The fit is given by $F = F_0 + B/(t_0 - t)^\alpha$ with $t_0 \approx 0.0863$, $B \approx 0.000806$, $\alpha \approx 0.879$, subtracted background $F_B \approx 13.96088$, a residual flux constant $F_0 \approx -0.0171$.

phase is clearly explosive and can be accurately fit by the following function (Fig. 13):

$$F = F_0 + B/(t_0 - t)^\alpha$$

with $t_0 \approx 0.0863$, $B \approx 0.000806$, $\alpha \approx 0.879$, and a residual flux $F_0 \approx -0.0171$. Note that apart from this last constant, the background value $F_B \approx 13.9609$ has been subtracted from the total flux. By contrast with the initial phase, the local flux excess grows to a value $\gtrsim 1$ before the merger occurs, and the total flux then drops abruptly to its background value.

VII. CONCLUSIONS

The Phillips's staircase [4] has long since outgrown its original context. Indeed, it is of general interest as an outcome of the nonlinear scale and pattern selection processes in systems with an homogeneously mixed conserved density. The present paper is devoted to numerical studies and analysis of a limiting case of SC model recently introduced in Ref. [13], in the context of geostrophic fluids and magnetized plasmas. It evolves the potential vorticity (PV) and potential enstrophy with a versatile model of mixing set by the Rhines scale. The model controls enstrophy production by the PV gradient, additional independent pumping, and nonlinear damping. These system properties render it bistable, which is the key to SC formation.

The main results of the current investigation of this model can be summarized as follows:

- (1) Parameter regimes and mixing length scalings in which the staircases occur are analytically constrained to satisfy $l_0^2/l^2 = (1 + l_0^2/l_R^2)^\kappa$, $\kappa > 1$, where l_R is the Rhines scale $l_R^2 = \varepsilon/Q_y^2$
- (2) SC formation and their properties and stability were studied numerically, for differing parameters and boundary conditions
- (3) Analytic solutions for steady-state SC configurations are obtained and categorized into periodic and isolated (compact) type solutions
- (4) The time of persistence of a quasistationary SC configuration is demonstrated to depend entirely on its proximity to the closest stationary solution
- (5) SC mergers are studied and the likelihood of the next merger event is elucidated, again, from the perspective of the configuration's proximity to the closest periodic solution
- (6) Merger dynamics is identified as explosive in time, and localized in space to a pair of SC neighboring elements (steps or jumps)
- (7) Step mergers produce localized bursts of PV mixing and transport
- (8) Analytic solutions provide insight into the metastationary SC structures beyond the capability of numerical integration.

While metastationary SC configurations, which persist practically unchanged between the merger events, can be fully understood using analytic solutions, merger dynamics requires further quantitative studies. In this paper, we give only a phenomenological account of SC merging. We note that recovering mergers and understanding merger dynamics are somewhat problematic. Mergers are observed in numerical solutions of the basic hydrodynamic equations [34] and in models [13,35] but not in gyrokinetic simulations [25] of magnetic confinement plasmas. We briefly discuss applications to confinement below.

A. Applications to Magnetic Confinement

Potential vorticity (PV), central to this study, is also a useful analog of charge density in drift wave (DW) turbulence in plasmas. Indeed, the close analogy between PV and quasigeostrophic turbulence in fluids and DW turbulence in plasmas is discussed at length in Refs. [18,36]. The DW-driven transport is regulated by zonal flows (ZF), which, in turn, are driven by DWs [14,18,36]. ZFs are a key transport inhibitor in the fusion confinement devices, because they are almost undamped and produce no transport ($n = 0$) streaming across the density-temperature gradient. They coexist with the other two turbulent transport phenomena: avalanches and turbulence pulses. By contrast to the ZFs they are intermittent and require description beyond one dimension, but equally mesoscopic.

The SC merger studied in this paper is a connection point between the ZF-SC structures and the nonlinearly excited 2D avalanches and turbulence pulses.

Another point of special interest associated with even the simplest SC configuration, as shown, e.g., in Fig. 4, is its similarity to the temperature and density distributions in H-mode (high confinement regime) operation of magnetic fusion devices. The region at the left boundary with a steep gradient of the transported (by turbulence) quantity (Q in this case) is characterized by transport reduction associated with the low turbulence level (ε here). These steep gradient layers are called transport barriers. We see that a staircase may be thought of as a lattice of transport barriers, which is a type of confinement regime. Such arrays of shear layers have been observed in tokamak experiments [23].

This paper has elucidated in depth the basic physics of the ‘‘Hasegawa-Mima’’ [37–39] staircases, in which fluctuations are produced by external stirring, and which makes no distinction between density and potential (i.e., $\tilde{n}/n_0 = |e|\hat{\phi}/T_e$ for $m \neq 0$ fluctuations). A more interesting case is the ‘‘Hasegawa-Wakatani’’ [40] staircase, for which

- (1) Density and potential evolve separately, but are coupled.
- (2) Drift wave instability processes allow access to free energy and promote the growth of vorticity flux at the expense of particle flux.
- (3) Consistent with (2), vorticity and particle fluxes are dynamically coupled
- (4) Spontaneous transport barrier formation is possible.

SC formation in the Hasegawa-Wakatani system are discussed in Refs. [13,14]. These studies are primarily computational. Further analysis will be coming in a future publication.

ACKNOWLEDGMENTS

We thank G. Dif-Pradalier, Y. Hayashi, D. W. Hughes, and W. R. Young for helpful discussions. P.H.D. acknowledges useful conversations with participants in the 2015 and 2017 Festival de Theorie, the 2018 Chengdu Theory Festival, and the 2014 Wave-Flows Program at KITP. This research was supported by the Department of Energy under Award No. DE-FG02-04ER54738.

APPENDIX A: STAIRCASE PARAMETERS

An extremum condition for Eq. (10), $F'(\xi) = 0$, contains only one parameter, ε_0 , and can be written as

$$(\xi + 1)^3 - 2\varepsilon_0\xi = 0.$$

It is convenient to write the solution of this cubic equation in a trigonometric form. The two positive roots $\xi_{0,1}$ are given by

$$\xi_n = 2\sqrt{\frac{2\varepsilon_0}{3}} \sin \left[\frac{1}{3} \sin^{-1} \left(\frac{3}{2} \sqrt{\frac{3}{2\varepsilon_0}} \right) + \frac{2}{3} \pi n \right] - 1, \quad n = 0, 1. \quad (\text{A1})$$

From this expression, we obtain a condition for the existence of the two isolated roots $\xi_{0,1}$, namely, $\varepsilon_0 > 27/8$ (the third roots is irrelevant here). Another requirement for the bistability is imposed on Q_y by the two relations in Eq. (11). However, this constraint is not precise in that Q_y also changes in the transition from one stable state to the other, along with ξ . At the same time, one can easily determine $Q_y(\xi)$ variation by assuming that it changes in space but remains stationary. This assumption relates Q_y to ξ by the constant diffusive flux in Eq. (6). It is totally justified for quasistationary phases of the SC evolution (Sec. V).

APPENDIX B: COMPARISON BETWEEN ANALYTICAL AND NUMERICAL SOLUTIONS

Periodic analytic solutions with small conventional diffusivity and a moderate number of total steps are characterized by the values E and b that are very close to their separatrix values E_* and

b_* [Eqs. (15) and (16)]. This results in extended flat parts of the $\psi(y)$ profile in Fig. 9 and those of ε and Q_y , shown earlier in Fig. 4. That $E \approx E_*$, is also obvious from the expression for the SC period in Eq. (19). On writing it as $\mathcal{L} = I(E)/L$ and noting that $L \gg 1$ and $\mathcal{L} \sim 1$, we find that $I \gg 1$ which implies $E \approx E_*$ [recall that $\max W(\psi) = E_*$]. Moreover, since $I \sim \ln(E_* - E)^{-1}$ and $L \approx 48$ in this particular run, E may, in principle, become close to E_* to the machine accuracy, because $E_* - E \sim \exp(-L)$. By examining the numbers we find that the difference between the numerical and analytical values of $\min \psi(y)$, shown in Fig. 9 is $\sim 10^{-4}$. This result implies that $E_* - E \sim 10^{-8}$ which is not inconsistent with the above estimate of the logarithm of this quantity.

-
- [1] L. Prandtl, *Essentials of Fluid Dynamics: With Applications to Hydraulics, Aeronautics, Heteorology and Other Subjects* (Blackie & Son, London, 1953).
- [2] J. Pedlosky, *Geophysical Fluid Dynamics* (Springer Science & Business Media, New York, 2013).
- [3] P. B. Rhines and W. R. Young, Homogenization of potential vorticity in planetary gyres, *J. Fluid Mech.* **122**, 347 (1982).
- [4] O. M. Phillips, Turbulence in a strongly stratified fluid – is it unstable? *Deep-Sea Res. Oceanogr. Abstr.* **19**, 79 (1972).
- [5] F. L. Hinton, Thermal confinement bifurcation and the L- to H-mode transition in tokamaks, *Phys. Fluids B* **3**, 696 (1991).
- [6] J. D. Murray, *Mathematical Biology. II Spatial Models and Biomedical Applications, Interdisciplinary Applied Mathematics*, Vol. 18 (Springer-Verlag New York, New York, 2001).
- [7] V. B. Lebedev and P. H. Diamond, Theory of the spatiotemporal dynamics of transport bifurcations, *Phys. Plasmas* **4**, 1087 (1997).
- [8] M. A. Malkov and P. H. Diamond, Analytic theory of L-H transition, barrier structure, and hysteresis for a simple model of coupled particle and heat fluxes, *Phys. Plasmas* **15**, 122301 (2008).
- [9] E. Knobloch, Spatial localization in dissipative systems, *Annu. Rev. Condens. Matter Phys.* **6**, 325 (2015).
- [10] D. G. Dritschel and M. E. McIntyre, Multiple jets as PV staircases: The phillips effect and the resilience of eddy-transport barriers, *J. Atmos. Sci.* **65**, 855 (2008).
- [11] P. B. Rhines, Jets, *Chaos* **4**, 313 (1994).
- [12] N. J. Balmforth, S. G. L. Smith, and W. R. Young, Dynamics of interfaces and layers in a stratified turbulent fluid, *J. Fluid Mech.* **355**, 329 (1998).
- [13] A. Ashourvan and P. H. Diamond, On the emergence of macroscopic transport barriers from staircase structures, *Phys. Plasmas* **24**, 012305 (2017).
- [14] T. S. Hahm and P. H. Diamond, Mesoscopic transport events and the breakdown of fick's law for turbulent fluxes, *J. Korean Phys. Soc.* **73**, 747 (2018).
- [15] F. Wagner *et al.*, Regime of Improved Confinement and High Beta in Neutral-Beam-Heated Divertor Discharges of the ASDEX Tokamak, *Phys. Rev. Lett.* **49**, 1408 (1982).
- [16] K. H. Burrell, Effects of E x B velocity shear and magnetic shear on turbulence and transport in magnetic confinement devices, *Phys. Plasmas* **4**, 1499 (1997).
- [17] J. W. Connor and H. R. Wilson, A review of theories of the L-H transition, *Plasma Phys. Controlled Fusion* **42**, 1 (2000).
- [18] P. H. Diamond, S.-I. Itoh, K. Itoh, and T. S. Hahm, Zonal flows in plasma -a review, *Plasma Phys. Controlled Fusion* **47**, 35 (2005).
- [19] X. Garbet, Introduction to drift wave turbulence modelling, *Fusion Sci. Technol.* **53**, 348 (2008).
- [20] L. Schmitz, L. Zeng, T. L. Rhodes, J. C. Hillesheim, E. J. Doyle, R. J. Groebner, W. A. Peebles, K. H. Burrell, and G. Wang, Role of Zonal Flow Predator-Prey Oscillations in Triggering the Transition to h-Mode Confinement, *Phys. Rev. Lett.* **108**, 155002 (2012).
- [21] G. Tynan *et al.*, Turbulent-driven low-frequency sheared E x B flows as the trigger for the H-mode transition, *Nucl. Fusion* **53**, 073053 (2013).

-
- [22] K. Ghantous and O. D. Gurcan, Wave-number spectrum of dissipative drift waves and a transition scale, *Phys. Rev. E* **92**, 033107 (2015).
- [23] G. Dif-Pradalier, G. Hornung, P. Ghendrih, Y. Sarazin, F. Clairet, L. Vermare, P. H. Diamond, J. Abiteboul, T. Cartier-Michaud, C. Ehrlacher, D. Estève, X. Garbet, V. Grandgirard, Ö. D. Gürcan, P. Hennequin, Y. Kosuga, G. Latu, P. Maget, P. Morel, C. Nordsieck, R. Sabot, and A. Storelli, Finding the Elusive ExB Staircase in Magnetized Plasmas, *Phys. Rev. Lett.* **114**, 085004 (2015).
- [24] Y. Kosuga and P. H. Diamond, Drift hole structure and dynamics with turbulence driven flows, *Phys. Plasmas* **19**, 072307 (2012).
- [25] G. Dif-Pradalier, P. H. Diamond, V. Grandgirard, Y. Sarazin, J. Abiteboul, X. Garbet, P. Ghendrih, A. Strugarek, S. Ku, and C. S. Chang, On the validity of the local diffusive paradigm in turbulent plasma transport, *Phys. Rev. E* **82**, 025401(R) (2010).
- [26] R. Wang, P. Keast, and P. Muir, A comparison of adaptive software for 1D parabolic PDEs, *J. Comput. Appl. Math.* **169**, 127 (2004).
- [27] Discussion of the drift-wave applications of this model in magnetically confined plasmas is also given in Refs. [13,14].
- [28] G. I. Taylor, Eddy motion in the atmosphere, *Philos. Trans. R. Soc. London A* **215**, 1 (1915).
- [29] P. B. Rhines, Waves and turbulence on a beta-plane, *J. Fluid Mech.* **69**, 417 (1975).
- [30] P.-C. Hsu, P. H. Diamond, and S. M. Tobias, Nonperturbative mean-field theory for minimum enstrophy relaxation, *Phys. Rev. E* **91**, 053024 (2015).
- [31] P. Goldreich and S. Sridhar, Magnetohydrodynamic turbulence revisited, *Astrophys. J.* **485**, 680 (1997).
- [32] A. Beresnyak and A. Lazarian, Scaling laws and diffuse locality of balanced and imbalanced magnetohydrodynamic turbulence, *Astrophys. J. Lett.* **722**, L110 (2010).
- [33] The compact solutions technically require an infinite integration domain, but can be reproduced in a finite domain with exponential accuracy (see also below).
- [34] K. Srinivasan and W. Young, Zonostrophic instability, *J. Atmos. Sci.* **69**, 1633 (2012).
- [35] A. Ashourvan and P. H. Diamond, How mesoscopic staircases condense to macroscopic barriers in confined plasma turbulence, *Phys. Rev. E* **94**, 051202(R) (2016).
- [36] Ö. D. Gürcan and P. H. Diamond, Zonal flows and pattern formation, *J. Phys. A* **48**, 293001 (2015).
- [37] A. Hasegawa and K. Mima, Pseudo-three-dimensional turbulence in magnetized nonuniform plasma, *Phys. Fluids* **21**, 87 (1978).
- [38] R. Z. Sagdeev, V. D. Shapiro, and V. I. Shevchenko, Convective cells and anomalous plasma diffusion, *Fizika Plazmy* **4**, 551 (1978) [*Sov. J. Plasma Phys.* **4**, 306 (1978)].
- [39] J. B. Parker and J. A. Krommes, Zonal flow as pattern formation, *Phys. Plasmas* **20**, 100703 (2013).
- [40] A. Hasegawa and M. Wakatani, Self-Organization of Electrostatic Turbulence in a Cylindrical Plasma, *Phys. Rev. Lett.* **59**, 1581 (1987).